ACS APPLIED MATERIALS & INTERFACES

www.acsami.org

Research Article

Ultrasensitive Fluorescent miRNA Biosensor Based on a "Sandwich" Oligonucleotide Hybridization and Fluorescence Resonance Energy Transfer Process Using an Ln(III)-MOF and Ag Nanoparticles for Early Cancer Diagnosis: Application of Central Composite Design

Ahmad Afzalinia and Mahdi Mirzaee*

Cite This: https://dx.doi.org/10.1021/acsami.0c00891

Read Online

ACCESS | Metrics & More | Article Recommendations | Supporting Information

ABSTRACT: Herein, a novel, rapid, highly sensitive, and selective fluorescent biosensor is presented, which is designed based on "sandwich-type" hybridization of oligonucleotides and the fluorescence resonance energy transfer (FRET) strategy. It senses and determines the MicroRNA-155 (miRNA-155) expression levels as a cancer biomarker. In this study, a modified La(III)-metal−organic framework(MOF) and silver nanoparticles (Ag NPs) were used as the energy donor−acceptor pairs in fluorescence quenching through the FRET process. La(III)-MOF was synthesized and then modified by glutaraldehyde as a cross-linking agent. The Ag NPs were also prepared, and then, the surface of both was conjugated with different 5′-amino-labeled ssDNA strands (aptamers). These prepared nanoprobes were characterized by various physicochemical techniques such as X-ray diffraction, energy-dispersive X-ray spectrometry, Fourier transform infrared, field emission scanning electron microscopy, UV−vis spectroscopy, elemental mapping, and gel electrophoresis. To optimize the detection conditions, several factors affecting biosensor performance were assessed by one variable-at-a-time and central composite design methods. Under optimum conditions, this "turn-off" fluorescent biosensor could detect and determine as low as 0.04 ppb (ng. mL^{-1}) or 5.5 fM of the miRNA-155 biomarker. Therefore, this biosensor provides highly promising potential for lung and breast cancer diagnosis.

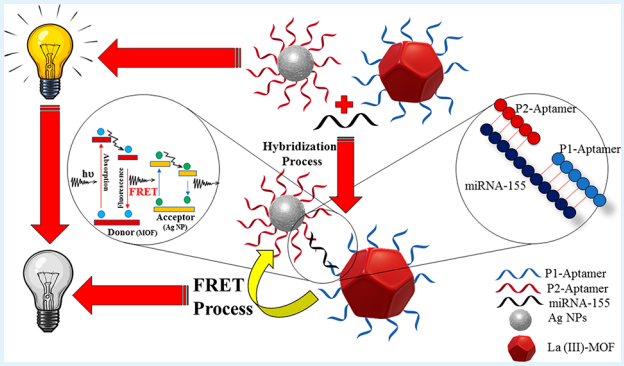

KEYWORDS: *MOFs, MicroRNA-155, biosensor, FRET, central composite design*

INTRODUCTION

Early cancer diagnosis incredibly improved the possibilities of efficient treatment and saved the lives of cancer patients. Consequently, a lot of effort and expenses have been dedicated to the research, development, and exploration of new methodologies to achieve a quick and early diagnosis of cancer signs.[1−3] Successful implementation of cancer identification and detection by conventional methods should entail extensive training and experience. Hence, rapid alternative and accurate approaches for cancer detection have emerged to overcome the existing restrictions. These efforts have led to emerging and developing noninvasive cancer diagnosis methods as powerful tools for clinical usage.[4−6] Accordingly, biosensors for chemical sensing of cancer biomarkers have recently promoted as promising and noteworthy alternatives to existing conventional cancer detection methods.[7]

The cancer markers are maybe some molecules produced by tumor cells or specific responses or behavior of the body's defense system to the presence of cancer. These biomarkers can include an extensive range of biochemical substances such as micro-ribonucleic acids (frequently abbreviated to miRNAs), proteins, small metabolites, and cytogenetic and cytokinetic parameters that exist in all tumor cells.[8−10] Over the past decade, several biological abnormalities have been observed in the blood plasma of cancer patients, such as unexpected changes in the expression level of some miRNAs. Short noncoding RNA strands, which are 18 to 24 nucleotides long, are known as vital regulators in the expression of target genes at the post-transcriptional level via translational repression or destruction of "messenger"-type RNA molecules (mRNAs).[11−13] These miRNAs are an essential subcategory of RNA molecules that play notable roles in various metabolic and biological processes such as differentiation, development, proliferation, apoptosis, and angiogenesis. Also, they have recently attracted plenty of attention because of their potential

Received: January 15, 2020
Accepted: March 6, 2020

Scheme 1. Schematic Diagram of Photoluminescence Quenching-Based Detection of miRNA-155 as a Cancer Biomarker by the FRET Process

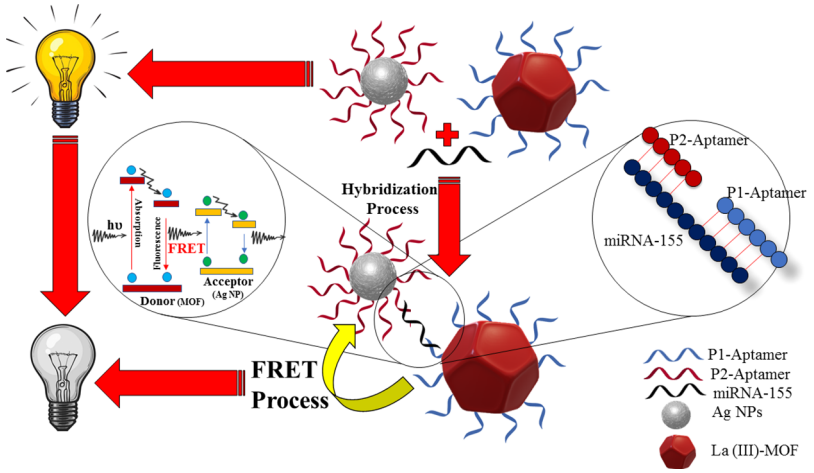

as a biomarker in cancer diagnosis.[14−16] To detect the miRNA strands, three laboratory methods were applied traditionally, including microarrays,[17] reverse transcription polymerase chain reaction,[18] and northern blotting.[19] However, these methods are time-consuming or expensive processes.[20] So far, several strategies and platforms have been employed to design a biosensor for miRNA detection based on surface-enhanced Raman spectroscopy,[21] electrochemical technique,[22−26] fluorescence spectroscopy,[27,28] surface plasmon resonance,[29,30] and so on. Among these, fluorescence-based methods have been considered as promising ways because of their natural high sensitivity, rapidity, and simplicity.[31,32] Therefore, a wide range of different materials, such as noble metallic nanoparticles,[33] graphene-based nanomaterials,[34,35] and semiconductor quantum dots,[36] were used to develop this method.

In the last decade, utilization of metal−organic frameworks (MOFs) in the field of optical sensors, especially fluorescence-based sensors, have grown very rapidly.[37−41] The term "MOFs" refers to a novel class of hybrid crystalline materials that exhibit exceptional advantages and features such as high and tunable porosity, large surface area (over 7000 $m^2 \cdot g^{-1}$), modifiable chemical functionality, and excellent thermal (or mechanical) stabilities.[42,43] Thus, they are widely employed in heterogeneous catalysis, gas storage and separation, semiconductors, proton conduction, chemical sensing, energy storage, and drug delivery.[44] MOFs, as indicated by the name, can merely self-assemble from their corresponding inorganic part (metal ions or polynuclear clusters) and organic bridging linkers that often contain aromatic or conjugated π moieties. Therefore, their optical properties, in general, and their luminescence behavior, especially, could be originated from both metal and organic components and could conveniently be tuned through the interactions among these building units.[42] The fluorescent MOFs, besides their exceptional surface areas and because of special combination of their inorganic and organic photonic units, could make profound chemical sensors endowed with superior performance. The acquired evidence reveals their unique properties and benefits such as reusability, rapid response, high sensitivity, and high selectivity.[45]

In 2007, Rieter and co-workers demonstrated that a lanthanide-based MOF could be employed for the luminescent detection of dipicolinic acid for the first time.[46] However, the primary utilization of MOFs as a platform for fluorescent biosensors is reported by Chen's group, who synthesized a two-dimensional Cu-based MOF and applied it to detect the HIV-1 DNA sequences and thrombin.[47] The majority of luminescence-based MOF sensors for DNA or RNA strands operate through a turn-off strategy, which in the turn-off state, the fluorophore-labeled single-stranded DNA (ss-DNA) probes adsorb onto the surface of the MOF and quench the luminescence of the fluorophore through a photo-induced electron-transfer process. The ss-DNA or RNA, known as aptamers or bioprobes, could bind to specific targets via folding into different secondary and tertiary structures.[48] In the presence of a target, which is the complementary strand of the probe, the hybridization process that forms a double-stranded DNA (ds-DNA) and releases it from the surface of MOF occurs. This recovers the fluorescence intensity of the fluorophore (the turn-on state).[42] In this strategy, probable recapturing of the formed ds-DNAs may lead to the fake detection signals. To reduce the false signals, the "sandwich-DNA" hybridization strategy was developed, in which there is a pair of energy donor−acceptor probes that are used for biomarker sensing according to the fluorescence resonance energy transfer (FRET) process. To the best of our knowledge, this study is the first research in the utilization of MOFs and metallic nanoparticles with this method. Numerous types of biosensing platforms based on luminescence quenching ability of metallic nanoparticles, especially silver and gold, have been successfully utilized for the detection and identification of different classes of biomarkers such as nucleic acids, antigens, and proteins as targets. Noble metal nanostructures were considered to be the ideal fluorescent quencher for luminescent sensors.[49] It was known that the unique luminescence quenching ability of noble metal nanoparticles is derived from localized surface plasmon resonance. When an incoming photon hits a spherical metallic nanoparticle surface, the photon's energy is absorbed by conduction electrons that are located near the surface of the nanostructure. A schematic of the working principle for the designed biosensor and FRET process is presented in Scheme 1.

It was known that the number of aptamers linked to the surface of probes directly impacts the performance of the hybridization process and determines the detection limit of miRNA sensing. Therefore, MOFs with a high surface area

https://dx.doi.org/10.1021/acsami.0c00891
ACS Appl. Mater. Interfaces XXXX, XXX, XXX−XXX

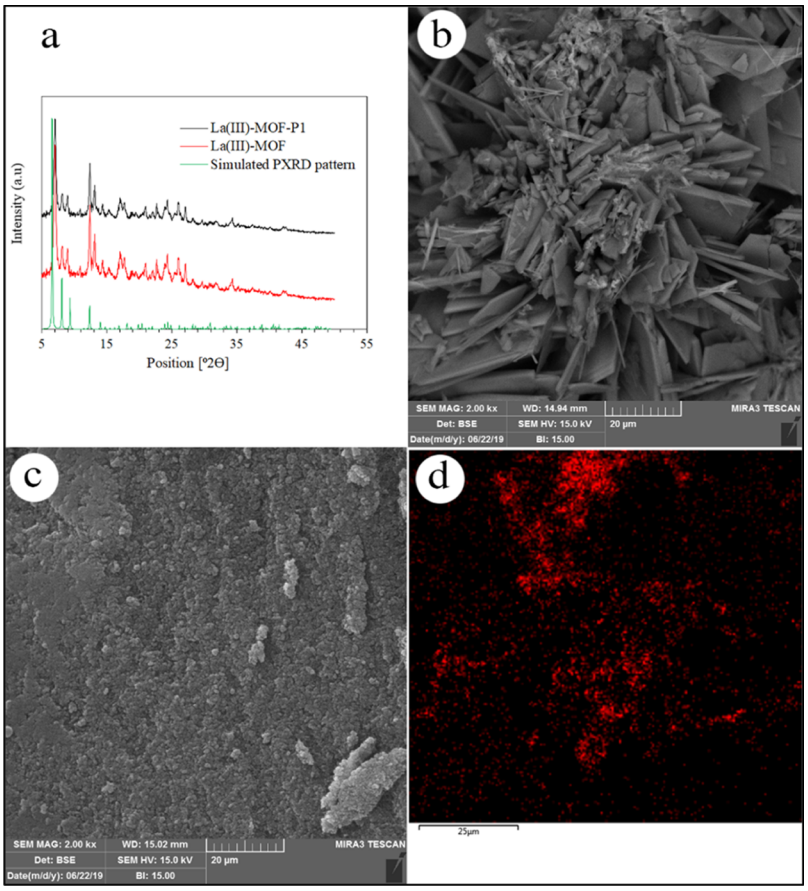

Figure 1. (a) XRD patterns of stimulated and as-prepared La(III)-MOF and La(III)-MOF-P_1, (b) FESEM image of La(III)-MOF, (c) FESEM image of La(III)-MOF-P1, and (d) phosphorus mapping of La(III)-MOF-P1.

would be good candidates for effective preconcentration of targets which significantly improve the sensing performance. The designed biosensor has been implemented to detect trace amounts of MicroRNA-155 (miRNA-155) as lung cancer (also known as bronchogenic carcinomas) and breast cancer biomarkers in real samples. These two types of cancers are responsible for the many human fatalities worldwide every year. Recent studies have shown that miRNA-155 unusually expressed and existed in biological fluid samples of breast or lung cancer patients.[50]

The performance of biosensors affectedly depends on the hybridization process and duplex strand formation between target miRNA and probes, and there are a large number of parameters that influence it. Therefore, traditional one-factor-at-a-time technique is not a suitable choice to optimize the conditions of this hybridization reaction because it completely ignores the interactions of several factors. The design of experiments is described as a strategy to plan the research studies and optimize the process conditions using multivariable statistic methods. However, it has been rarely used in oligonucleotide detection using the fluorescence biosensor.[51] In this study, we also report the application of response surface methodology (RSM) to predict the optimal experimental conditions in miRNA-155 detection with the designed biosensor to maximize the hybridization signal.

EXPERIMENTAL SECTION

The amino-functionalized La(III)-MOF[52] and silver nanoparticles (Ag NPs)[53] were prepared according to the literature reports. DNA aptamer probes (P1: 3′-$(CH_2)_6$-NH-AUCACGAUUAGCAUUAA-5′ and P2: 3′-ACCCCU-NH-$(CH_2)_6$-5′) and miRNA target oligonucleotides were purchased from Bioneer company (South Korea). The real sample miRNA-155 was supplied by the hematology and oncology center of Kousar hospital (Semnan, Iran). The details of experimental procedures are reported in the Supporting Information.

Optimization of Biosensing Conditions. To optimize the sensing conditions for miRNA detection and enhance the performance of the designed biosensor, various parameters such as pH, concentration of miRNA-155 (ppb), level of probe-1 (ppb), time of hybridization (min), level of probe-2 (ppb), and temperature (°C), which could influence the efficiency of biomarker sensing, were screened with a Plackett−Burman design (see the Supporting Information file). In the next step, the one factor-at-a-time method and central composite design (CCD) were employed to optimize the sensing conditions.

RESULTS AND DISCUSSION

Preparation and Characterization of Probe-1 (La(III)-MOF-P1). The powder X-ray diffraction (XRD) patterns of La(III)-MOF, before and after immobilization of probe-1 on its surface, are shown in Figure 1a. These XRD patterns show excellent agreement with the simulated XRD pattern from CCDC 776748.[52] It also indicates that the host framework of La(III)-MOF does not disturb during the DNA immobilization process. Energy-dispersive X-ray spectroscopy (EDS) was used for identifying the elemental composition of the as-prepared La(III)-MOF. The presence of La, C, O, and N atoms in it was certified, as shown in Figure S1 and Table S1.

https://dx.doi.org/10.1021/acsami.0c00891
ACS Appl. Mater. Interfaces XXXX, XXX, XXX−XXX

Fourier transform infrared (FT-IR) spectroscopy was also applied to characterize the structure of the as-prepared and modified La(III)-MOF (Figure S2). In the FT-IR spectrum of the as-prepared La(III)-MOF, the characteristic peaks of the ligand were changed, which evidenced the successful synthesis of the so-called MOF. Symmetric and asymmetric stretching vibrations of N−H at 3506 and 3393 cm^{-1} in the ligand[54] were moved to 3460 and 3375 cm^{-1} in the as-prepared La(III)-MOF.[52] In the ligand spectrum, an absorption band that appeared at 1690 cm^{-1} could be assigned to the N−H bending vibration[54] that moved to 1673 cm^{-1} in the as-prepared La(III)-MOF.[52] The weak band at 2930 cm^{-1}, which correspond to aromatic C−H stretching vibrations of ligands, did not change in the as-prepared La(III)-MOF spectrum. Also, the peak of the protonated carboxylic group was not observed between 1680 and 1715 cm^{-1}. After modification of the La(III)-MOF framework with glutaraldehyde, two sharp peaks with a particular shape assigned to the C−H stretching vibrations of glutaraldehyde appeared at 2908−2930 cm^{-1}. A peak at 1688 cm^{-1} that may attribute to the carbonyl group of glutaraldehyde was also seen. These observations confirmed the successful modification of the La(III)-MOF surface and the preparation of La(III)-MOF-G for the immobilization of aptamer P1. The amount of the adsorbed aptamer P1 was very low which did not change the FT-IR spectrum of La(III)-MOF-G.

Moreover, field emission scanning electron microscopy (FESEM) images of the as-prepared La(III)-MOF, La(III)-MOF-G, and La(III)-MOF-P1, shown in Figures 1b and S1a,c, respectively, showed that the morphology of La(III)-MOF-G and La(III) MOF-P1 is completely different from that of the as-prepared La(III)-MOF. These changes could be attributed to the linkage of glutaraldehyde and adsorption of aptamer P1 onto the surface of La(III)-MOF crystals.

The DNA building blocks comprise three parts. These include thymine, adenine, guanine, and cytosine bases or nucleotides which join together to form a strand of DNA by the phosphate and sugar groups. Therefore, phosphorus mapping of La(III)-MOF-P1 was used to evidence successful immobilization of DNA onto the surface of La(III) MOF-G (Figure 1d).

The fluorescence wavelength of La(III)-MOF, shown in Figure S3b, shifted a little after modification and adsorption of aptamer P1. This could also confirm the successful decoration of aptamer P1 onto the surface of La(III)-MOF.

Preparation and Characterization of Probe-2 (Ag NPs−P2). Preparation of colloidal Ag NPs was analyzed using UV−vis spectroscopy (Figure 2a). The prepared Ag NPs exhibit an absorption band with a maximum at 430 nm that relates to the surface plasmonic vibration.[51] According to the Mie theory, the extinction (or transmittance) spectrum can be employed to measure the size of metallic nanoparticles.[55] Figure 2b shows the obtained transmittance spectrum of the prepared Ag NPs that revealed 40−50 nm particles in this sample.[53]

The DNA aptamer P2 was used to bind the surface of Ag NPs, and UV−vis spectroscopy and agarose gel electrophoresis were performed to ensure its binding. In Figure S3a, the UV−vis spectrum of Ag NPs−P2 is a mixture of Ag NPs and the P2 aptamer. There is also a red shift in the absorption peak at around 435 nm which means the successful attachment of DNA aptamer P2 onto the surface of Ag NPs. Furthermore, the obtained results, from agarose gel electrophoresis (Figure 2c), reveal that the pure Ag NPs (lane 1) run faster than Ag NPs−P2 (lane 2) under completely identical conditions. It could be attributed to the larger size of the Ag NPs−P2, which penetrates the gel slower.[56] Therefore, it can be concluded that DNA aptamer P2 favorably immobilizes onto the surface of Ag NPs.

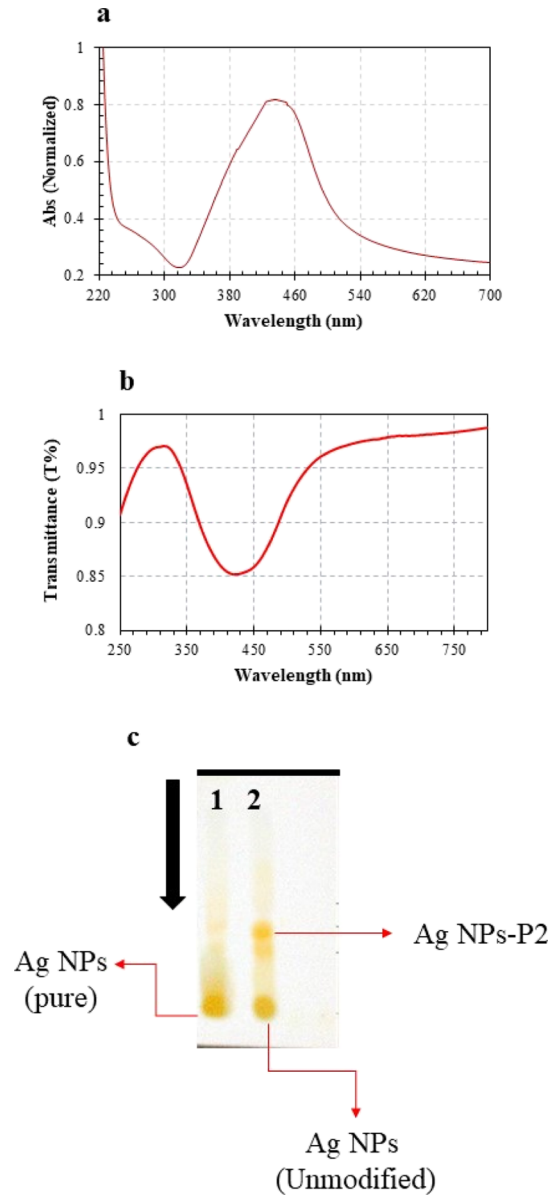

Figure 2. (a) UV−vis spectrum of the prepared Ag NPs, (b) transmission spectra of Ag NPs, and (c) agarose gel electrophoresis of Ag NPs (lane 1) and Ag NPs−P2 (lane 2).

Figure S3 also shows the fluorescence spectra of La(III)-MOF, miRNA-155, aptamer P1, and P2. Their comparison illustrated that the fluorescence intensity of La(III)-MOF is much higher than that of both aptamers and miRNA-155 and completely covers them.

Optimization of the Main Factors Affecting FRET. *Effect of the Initial Concentration of miRNA-155.* Figure 3a shows the quenching efficiency versus the miRNA-155 concentration level. This plot exhibits two different slopes with a continuous increase of the target concentration. These observations are due to the number of aptamers that immobilized on the surface of Ag NPs and La(III)-MOF.

https://dx.doi.org/10.1021/acsami.0c00891
ACS Appl. Mater. Interfaces XXXX, XXX, XXX−XXX

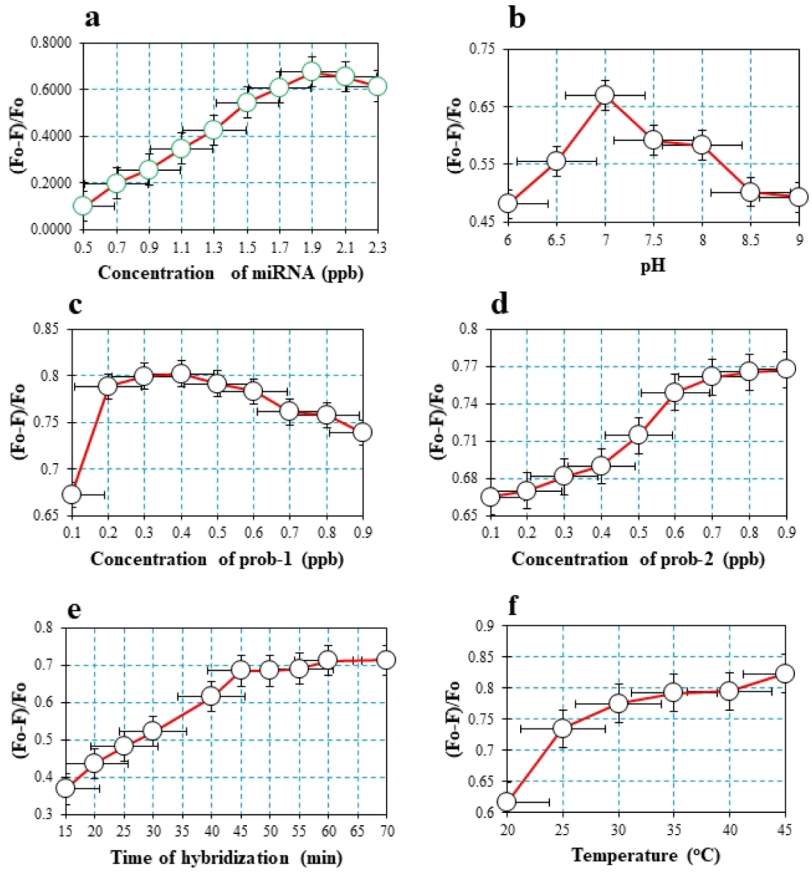

Figure 3. Impact of various factors on the biosensor response: effect of the (a) concentration of miRNA-155 (pH: 7, time: 30 min, temperature: 25 °C, and concentration of probe-1: 0.2 ppb and probe-2: 0.5 ppb), (b) pH (miRNA concentration: 1.9 ppb, time: 30 min, temperature: 25 °C, and concentration of probe-1: 0.2 ppb and probe-2: 0.5 ppb), (c) concentration of probe-1 (miRNA concentration: 1.9 ppb, pH: 7, time: 30 min, temperature: 25 °C, and probe-2: 0.5 ppb), (d) concentration of probe-2 (miRNA concentration: 1.9 ppb, pH: 7, time: 30 min, temperature: 25 °C, and probe-1: 0.4 ppb), (e) time (miRNA concentration: 1.9 ppb, pH: 7, temperature: 25 °C, and concentration of probe-1: 0.4 ppb and probe-2: 0.6 ppb), and (f) temperature (miRNA concentration: 1.9 ppb, pH: 7, time: 45 min, and concentration of probe-1: 0.4 ppb and probe-2: 0.6 ppb).

When miRNA-155 strands are introduced to the mixture of probe-1 and probe-2, up to 2 ppb, the numbers of available active sites are very higher than those of the target miRNA-155 strands, so the hybridization reaction and FRET process are quickly completed and quenching efficiency is high. However, by increasing the initial concentration of the target, their numbers became significant in comparison to the numbers of the available active sites and quenching efficiency decreased. In other words, the sensitivity of the biosensor in the 0.5−2 ppb range is more than that of the higher miRNA concentration level.

Effect of pH. The sequence pairing of target miRNA and probes through hydrogen bonding is significantly depended on pH.[52] In acidic conditions, protonation of bases disrupted hydrogen bonding and caused electrostatic repulsion between nucleotides. It might also destroy oligonucleotides; therefore, the hybridization process was performed at pH 6−9. Figure 3b indicates that maximum Q_E values were achieved in the pH range of 6.5−8. Therefore, neutral pH has been chosen in the continuation of this research.

Effect of the Probe Amount. The available sites for miRNA strands could be improved by increasing the number of probes. Hence, the effect of different amounts of probes (0.1−0.9 ppb) investigated to determine their impact on biosensor performance. According to Figure 3c, the fluorescence quenching efficiency increased immediately with increasing the amount of probe-1 from 0.1 to 0.2 ppb. Then, it remained constant from 0.2 to 0.4 ppb before starting to decrease, up to 0.9 ppb. Moreover, for the quencher probe-2, the fluorescence quenching efficiency increases with increasing concentration from 0.1 to 0.6 ppb (Figure 3d). Then, it almost remained constant up to 0.9 ppb. These observations explain that the excess number of probes makes a false response. When the number of fluorophore or quencher species is more than miRNA targets, incorrect biosensor responses were observed because of probe particle aggregation. Also, in the low levels of probes, the sensitivity of the biosensor significantly reduces because of the lack of enough probes for the hybridization process. When the amounts of probe-1 and probe-2 are 0.4 and 0.6 ppb, respectively, the maximum quenching efficiency for the system was achieved. Therefore, these amounts of probes were chosen as the optimum and used in subsequent experiments.

Effect of the Hybridization Time. The hybridization time is another main factor that affected the response in the miRNA-155 biosensing process. As shown in Figure 3e, the fluorescence quenching efficiency has enhanced with increasing hybridization time from 15 to 45 min and then almost remained unchanged. These results showed that at least 45 min was required for reaching the chemical equilibrium or

https://dx.doi.org/10.1021/acsami.0c00891
ACS Appl. Mater. Interfaces XXXX, XXX, XXX−XXX

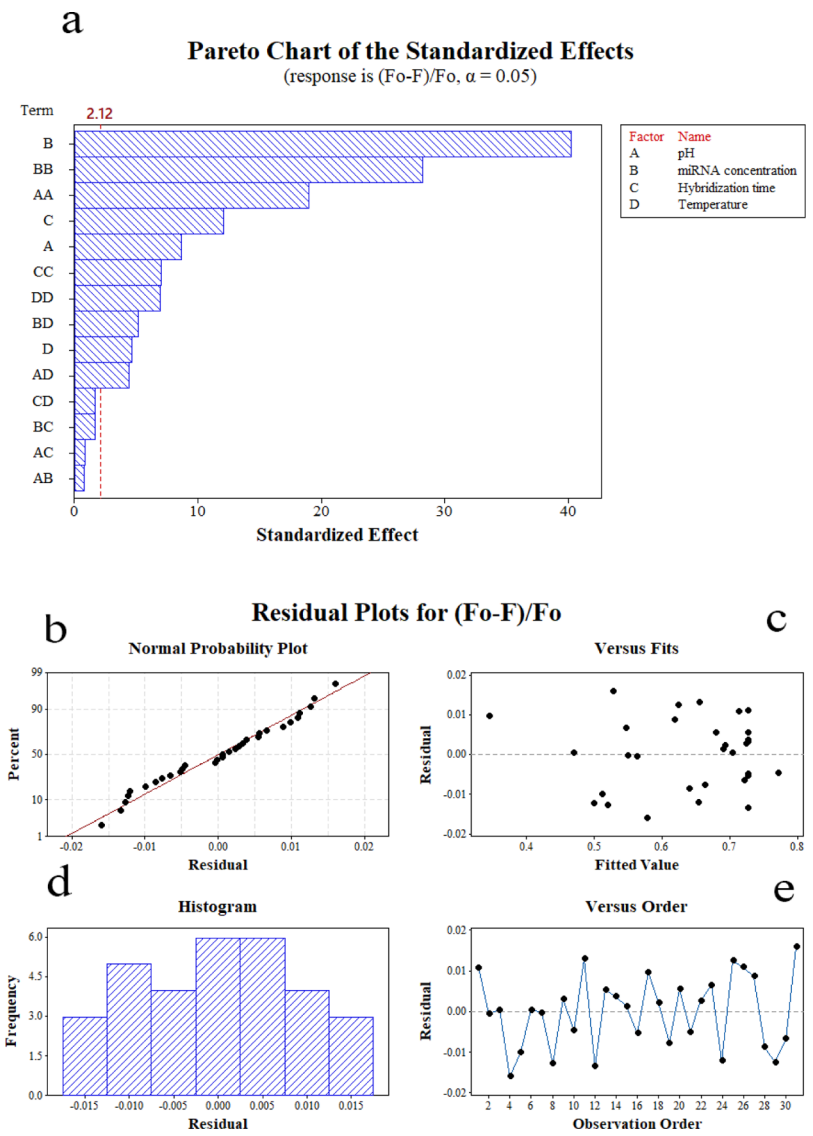

Figure 4. (a) Pareto plot for the determination of the main variables and investigation of the model adequacy by residual plots: (b) normal probability, (c) vs fits, (d) histogram, and (e) vs order.

occupation of active sites on probes, so 45 min was considered as the optimum time needed for mixing biomarker targets and probes.

Effect of Temperature. Because the temperature can change interactions between miRNA strands and probes, it has significantly impacted on the responses of the biosensor. Thus, the temperature was adjusted in the range of 20−45 °C to investigate its effect on miRNA-155 detection. As shown in Figure 3f, the response of the sensor increased by increasing the temperature up to 45 °C. A probable description is that increasing the temperature accelerates the hybridization process by further collision. However, the fluorescence intensity of La(III)-MOF may reduce at higher temperatures by improving the vibrational relaxation mechanism in which the collision between the solvent molecules and probe-1 particles resulted in the nonradiative relaxations.[57] Consequently, the temperature was set at 25−35 °C for obtaining the best real response.

The fluorescence spectra of sensor platforms under different conditions are given in Figure S4a−e, and Figure S4f illustrates the fluorescence quenching of this biosensor system in the optimum conditions obtained from one factor-at-a-time optimization experiments.

Experimental Design. The CCD, as the most common RSM, has been employed for deciding the impacts of different parameters and their interactions in miRNA-155 detection. The experimental factors, predicted results, runs, and their responses are listed in Table S5. At first, the statistical significance of these independent factors and related interactions has been investigated using a Pareto plot, as indicated in Figure 4a. According to this plot, the most significant independent variables and two factorial interactions between them were determined (A, B, C, D, A^2, B^2, C^2, $A \times D$, and $B \times D$), and then, the obtained experimental data were analyzed using the ANOVA technique. This technique is a robust statistical procedure that can be utilized to separate and estimate the different causes of variation. Therefore, ANOVA analysis can help us decide which factor has significantly impacted the response of the biosensor based on the diverse descriptive statistics, such as F-value, p-value, correlation coefficient (R^2), and adjusted correlation coefficient (R^2_{Adj}).

https://dx.doi.org/10.1021/acsami.0c00891
ACS Appl. Mater. Interfaces XXXX, XXX, XXX−XXX

In the first model analyzing step, the residual plots have been used to judge the model adequacy. The histogram plot (Figure 4d) exhibits a standard Gaussian distribution, and according to the versus order plot (Figure 4e), residuals represented no clear pattern around the zero line, which means there is no serial correlation between these data and residuals are independent of each other. The normal probability plot (Figure 4b) was also exhibited to have no deviations from a straight line, and the versus fits plot (Figure 4c) displayed that residuals were scattered shapeless and randomly around the zero line. These observations revealed that residuals have constant variance, and the obtained responses from the model have high adequacy.

Results of the ANOVA analysis are summarized in Table 1. The model is significant when its *p*-value and lack of fit, which were obtained by Fisher's exact test, were significant and insignificant, respectively. Hence, in 95% confidence intervals, the *p*-value should be lower than 0.05 and the lack of fit should be higher than 0.05. According to the obtained *F*-value (258.48), *p*-value ($p \leq 0.0001$), and *F*-value lack of fit (2.08), it could be ascertained that this model is hugely significant and it has the best adaptation to the responses. Furthermore, the adequacy and quality of the model can be explored with an investigation of the coefficient (R^2) values. Also, the proximity and agreement of the adjusted correlation coefficient (R^2_{Adj}) to the correlation coefficient (R^2) describe the unique ability of this quadratic model for the adjustment of theoretical values and experimental data. R^2, R_{Adj}^2, and R_{Pred}^2 were calculated to be 99.23, 98.85, and 97.72, respectively. According to these results, the adequacy of the quadratic model was approved for the detection of miRNA-155.

In addition, the mathematical relationship of the response on variables and their linear and quadratic interactions can be estimated with the following polynomial equation (based on regression coefficients and data analysis that are displayed in Table 2). Equation 1 is an adjusted model for significant factors (with the *p*-value lower than 0.05), affecting the response of the biosensor. Here *R* represents the fluorescence quenching efficiency, *A*, *B*, *C*, and *D* indicate the terms of the coded values of pH, miRNA-155 concentration, hybridization time, and temperature, respectively. Also, A^2, B^2, C^2, and D^2 are their quadratic terms. The interactions between the miRNA-155 concentration and temperature ($B \times D$) described a negative effect on response. $A \times D$ was significant, indicating that the interaction exists between pH and temperature. The pH and miRNA-155 concentration have the most significant impact on the response of the biosensor as designated by the positive terms in eq 1. Based on the collected results of the CCD method, we can decide that the effects of the interactions between factors were less than the influences of individual ones.

The 3D response surface plots were utilized to explain the role of significant variables and their mutual interactions. These plots illustrate the relevance between dependent factors and experimental levels of each independent factor. Data from Figure 5a demonstrated that higher quenching efficiency was obtained at room temperature around the neutral pH. Also, increases in miRNA-155 concentration at about room temperature lead to enhancement of the response of the biosensor (Figure 5b).

Table 1. Obtained Results of ANOVA of the Quadratic Models Predicted for Each Factor in the miRNA-155 Detection Process and Their Coefficient Values

source	DF	Adj SS	Adj MS	*F*-value	*p*-value
model	14	0.310853	0.022204	212.48	0.000[a]
linear	4	0.194286	0.048572	464.80	0.000[a]
pH	1	0.007794	0.007794	74.58	0.000[a]
miRNA concentration	1	0.169025	0.169025	1617.46	0.000[a]
hybridization time	1	0.015246	0.015246	145.89	0.000[a]
temperature	1	0.002221	0.002221	21.26	0.000[a]
square	4	0.110996	0.027749	265.54	0.000[a]
pH × pH	1	0.037529	0.037529	359.13	0.000[a]
miRNA concentration × miRNA concentration	1	0.082929	0.082929	793.57	0.000[a]
hybridization time × hybridization time	1	0.005127	0.005127	49.06	0.000[a]
temperature × temperature	1	0.005022	0.005022	48.06	0.000[a]
2-way interaction	6	0.005570	0.000928	8.88	0.000[a]
pH × miRNA concentration	1	0.000069	0.000069	0.66	0.427[b]
pH × hybridization time	1	0.000079	0.000079	0.75	0.398[b]
pH × temperature	1	0.002059	0.002059	19.70	0.000[a]
miRNA concentration × hybridization time	1	0.000280	0.000280	2.68	0.121[b]
miRNA concentration × temperature	1	0.002785	0.002785	26.65	0.000[a]
hybridization time × temperature	1	0.000298	0.000298	2.86	0.110[b]
error	16	0.001672	0.000105		
lack-of-fit	10	0.001263	0.000126	1.85	0.233[b]
pure error	6	0.000409	0.000068		
total	30	0.312525			
model summary					
S		R^2	R_{Adj}^2	R_{Pred}^2	
0.0102225		99.47%	99.00%	97.49%	

[a]Significant. [b]Insignificant.

Table 2. Regression Coefficients for Each Main Factor That Impacts the miRNA-155 Sensing Process

term	coef.	SE coef.	*T*-value	*p*-value
constant	0.78123	0.00414	188.75	0.000[a]
pH	−0.01802	0.00224	−8.06	0.000[a]
miRNA concentration	0.08392	0.00224	37.54	0.000[a]
hybridization time	0.02520	0.00224	11.28	0.000[a]
temperature	−0.00962	0.00224	−4.30	0.000[a]
pH × pH	−0.03623	0.00205	−17.69	0.000[a]
miRNA concentration × miRNA concentration	−0.05385	0.00205	−26.30	0.000[a]
hybridization time × hybridization time	−0.01339	0.00205	−6.54	0.000[a]
temperature × temperature	−0.01325	0.00205	−6.47	0.000[a]
pH × temperature	0.01134	0.00274	4.14	0.001[a]
miRNA concentration × temperature	−0.01319	0.00274	−4.82	0.000[a]

[a]Significant.

https://dx.doi.org/10.1021/acsami.0c00891
ACS Appl. Mater. Interfaces XXXX, XXX, XXX−XXX

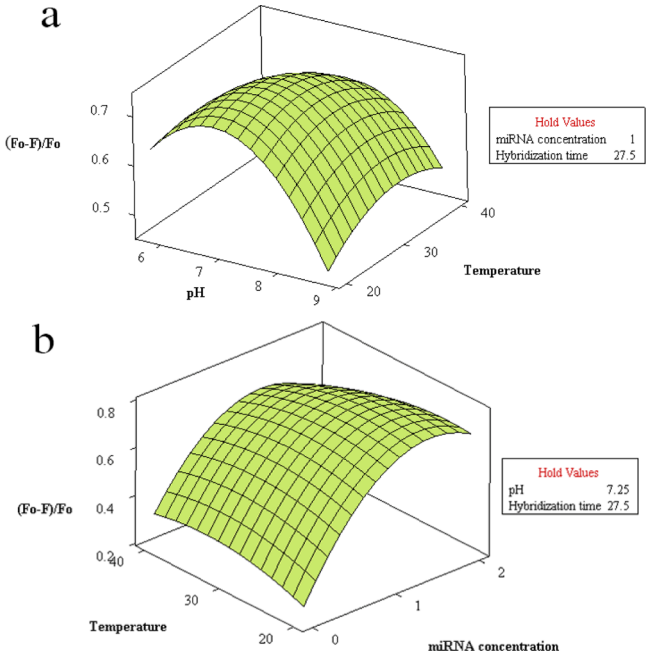

Figure 5. 3D response surfaces for biosensor response: (a) pH × temperature and (b) miRNA-155 concentration × temperature.

$$R = -2.853 + 0.8191A + 0.7570B + 0.006729C + 0.01323D - 0.06440A^2 - 0.21541B^2 - 0.000086C^2 - 0.000530D^2 + 0.003025A \times D - 0.00528B \times D \quad (1)$$

Finally, the CCD technique can predict the optimal conditions by a combination of main variables based on ridge maximum and canonical analysis. The optimum values of each significant factor (pH, miRNA-155 concentration, contact time, and temperature) that are predicted by the model are given in Table 3. Then, under the proposed optimal condition, the detection of miRNA-155 was performed and the response (0.7839) was compared with the predicted value from the CCD method eq 1 (0.7856). These results affirmed the feasibility, predictive ability, and adequacy of the suggested model.

Biosensor Performance Evaluation. The performance of the designed biosensor, for quantitative investigation and determination of miRNA-155, was evaluated further under optimal conditions achieved from the CCD method. As shown in Figure 6a, the analytical curve, which demonstrates the correlation between miRNA-155 concentration and fluorescence intensity ratios (F_0/F), is linear from 0.04 to 50 ppb with different slopes in two concentration ranges. These observations can be attributed to the aggregation of miRNA strands around active sites and occupancy of these sites. The calibration equations for the higher (1−50 ppb) and lower (0.04−0.1 ppb) miRNA-155 concentration ranges were calculated and could be indicated by $Q_E = 0.008\ C_{miRNA\text{-}155} + 0.4077$ ($R^2 = 0.9916$) and $Q_E = 3.3942\ C_{miRNA\text{-}155} + 0.0184$ ($R^2 = 0.9776$), respectively, where Q_E is the fluorescence

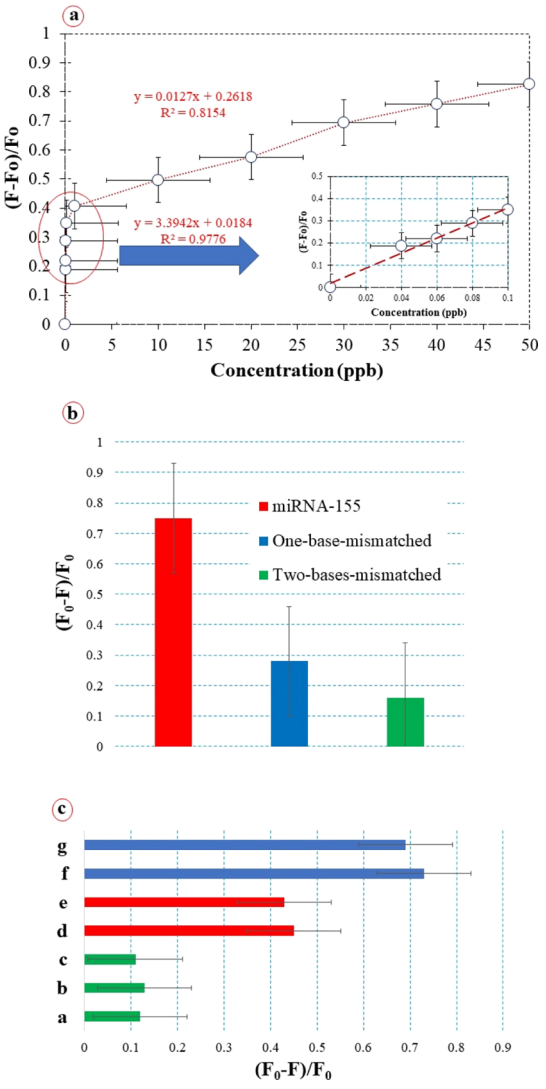

Figure 6. (a) Calibration curve (concentration range: 0.04−50 ppb), (b) specificity of the designed biosensor miRNA-155 (red), one-base-mismatched (blue) and two-bases-mismatched miRNA (green), and (c) responses of the biosensor for the detection of miRNA-155 in real samples [blank sample (a), healthy donors (b,c), lung cancer patients (d,e), and breast cancer patients (f,g)].

Table 3. Proposed Optimal Conditions and Predicated Response Derived by CCD

		multiple response and condition prediction			
		response $(F_0 - F)/F_0$			
variable	setting	fit	SE fit	95% CI	95% PI
pH	6.9621	0.7855	0.0052	(0.77473, 0.7964)	(0.7602, 0.8108)
miRNA concentration[a]	1.4545				
hybridization time[b]	39.3687				
temperature[c]	25.0505				

[a]ppb. [b]min. [c]°C.

https://dx.doi.org/10.1021/acsami.0c00891
ACS Appl. Mater. Interfaces XXXX, XXX, XXX−XXX

Table 4. Comparison of the Detection Performance of the Designed Biosensor with Some Recently Reported Methods for Detection of miRNA-155

	method	LOD	linear range	references
1	fluorescent detection	2.20 pM	1.00 pM to 10.00 nM	58
2	electrochemical	1.87 pM	5.60 to 5.60 \ 10^5 pM	59
3	electrochemical	0.32 fM	1.00 fM to 10.00 nM	60
4	electrochemiluminescence	0.67 pM	1.00 pM to 10.00 μM	61
5	fluorescent detection	11.00 pM	50.00 pM to 10.00 nM	62
6	fluorescent detection	33.40 fM	100.00 fM to 1.00 nM	63
7	fluorescent detection	100.00 pM	0.10 to 200.00 nM	27
8	fluorescent detection	5.20 fM	2.70 fM to 0.01 pM	this work

quenching and C represents the concentration of miRNA-155. The limit of quantitation and limit of detection (LOD) can be computed based on fluorescence intensity ratios from five measurements of the blank sample (eqs 2 and 3). These analytical parameters were estimated to be 0.04 ppb (or 5.21 fM) and 0.13 ppb (or 17.35 fM), for the miRNA-155 detection method.

$$\mathrm{LOQ} = \frac{10\sigma}{m} \tag{2}$$

$$\mathrm{LOQ} = \frac{3\sigma}{m} \tag{3}$$

where σ demonstrates the standard deviation of responses (fluorescence intensity ratios measured from blank samples) and m represents the slope of the calibration graph. The achieved LOD was comparable and moderately better than other reported fluorescence-based sensors for the detection of miRNA-155 as a lung or breast cancer marker. The detection performance of the designed biosensor was compared with some recently published articles, as shown in Table 4. In contrast to previous fluorescent methods, this biosensor provided the specific, quantitative, and sensitive detection method for miRNA-155 without the requirement for any amplification strategies such as enzymatic amplification of the signal or polymerase chain reaction (PCR).

To investigate and confirm the specificity and selectivity of the proposed platform for the biosensor, the detection and hybridization processes have been performed with miRNA-155 and single base and two base-mismatched miRNA strands for 1.50 ppb of each oligomer under identical conditions (Figure 6b). Accordingly, if mutated miRNA strands, as control sequences, are applied instead of miRNA-155, the fluorescence intensity ratio did not change considerably and very lower quenching was observed. This unique selectivity of the biosensor has been explained by the hybridization phenomenon and the formation of miRNA-probes heteroduplexes. As well known, the RNA strands only anneal to complementary DNA or RNA sequences; therefore, the sequences of the probes have been chosen to pair exclusively with miRNA-155.

The relative standard deviation (RSD) of response for different days can be used to demonstrate the reproducibility of the prepared biosensor,[64] which is an essential property for the practical applications. The calculated RSD of the biosensor in response to 1.50 ppb miRNA-155 was 4.46% for six tests, showing the excellent reproducibility of the biosensor.

Feasibility of the FRET Strategy. Based on the interaction between probe-1 and probe-2, fluorescence quenching may occur because of the FRET or inner filter effect (IFE) mechanism.[65] When the absorption spectrum of quencher species overlapped with both excitation and emission fluorophore spectra, the IFE mechanism may be responsible for the fluorescence quenching. It has been usually observed because of the shielding of the excitation beam, which highly depends on the concentration of quencher or fluorophore species in solution. However, when only the emission spectrum of the fluorophore overlapped with the absorption spectrum of quencher species, the emission of the fluorophore was absorbed by quencher species in the ground state. However, a prerequisite of this happening is that these species came together as close as 10−100 Å. At this condition, the fluorescence intensity was quenched by the FRET mechanism.[66,67] Figure S5a shows the UV−vis spectra of Ag NPs−P2 (probe-2, quencher species) and fluorescence excitation and emission of La(III)-MOF-P1 (probe-1, fluorophore species). It was seen that the absorption spectrum of probe-2 and the emission spectrum of probe-1 are completely overlapped, but the overlap between their absorption spectra is quite evident. Additionally, the Plackett−Burman design, as a beneficial technique for screening and searching the most efficient variables, shows that the concentration of Ag NPs−P2 is an insignificant parameter in the sensing process. Consequently, it would ensure that the suitable excited energy transfer from Ln(III)-MOF-P1 to Ag NPs−P2 by FRET is rather probable than that by the IFE mechanisms. Therefore, in the absence of miRNA-155, the fluorophore (probe-1) and quencher (probe-2) are far apart, resulting in insignificant FRET and high-intensity fluorescence detected (Figure S5b). However, by introducing miRNA-155, hybridization reaction brings the probes close together, which resulted in the significant FRET with an efficient quenching fluorescence signal (Figure S5c).

Real Sample Analyses. The applicability of the designed biosensor has been appraised by the detection of miRNA-155 expression levels in actual clinical samples with complex matrices that were collected from the hematology and oncology center of Kousar hospital (Semnan, Iran). For this purpose, human serum samples have been taken from patients with lung or breast cancer and also healthy persons (as a control). In the next step, miRNA-155 was isolated from blood plasma samples utilizing miRNeasy RNA isolation kits according to the Qiagen protocol. This process was precisely performed based on the standard procedure, which was explained in previous reports.[68] Figure 6c shows that serum samples of two healthy donors did not quench fluorescence intensity similar to the blank sample without the miRNA target. However, the fluorescence intensity completely quenched with serum samples of lung or breast cancer patients. Therefore, the designed FRET strategy can be successfully, effectively, and quantitatively employed to detect the upregulated expression of this cancer marker in real

https://dx.doi.org/10.1021/acsami.0c00891
ACS Appl. Mater. Interfaces XXXX, XXX, XXX−XXX

serums. These results indicate perfect agreement with previous reports that use the PCR technique for the detection of miRNA-155 in breast cancer patients.[68,69]

CONCLUSIONS

In summary, this research provides the most promising strategy for the detection of the miRNA-155 strand in clinical application. Accordingly, a robust biosensor was fabricated based on the FRET technique and "sandwich" hybridization process of the oligonucleotides. In this work, a simple, fast, and effective nanosensor was fabricated based on a fluorophore-quencher pair. A La(III)-MOF (as a fluorophore) and Ag NPs (as a quencher) were selected and then modified by specific aptamer strands for the designed strategy. The optimal conditions for sensing the miRNA-155 (target) achieved from the CCD method were pH, 6.9621; concentration of miRNA-155, 1.4545 ppb; contact times, 39.3687 min; and temperature, 25.0505 °C. Because of the result of ANOVA analysis (p-value < 0.0001 and lack of fit > 0.05), the high obtained values of R^2 (99.23), R_{Adj}^2 (98.85), and R_{Pred}^2 (97.72), and good agreement between them, the proposed model could significantly describe the sensing process with the best adaptation to the responses. High sensitivity (LOD 0.0386 ppb), high selectivity, and good applicability of this biosensor in real clinical serum are the advantages of this protocol.

ASSOCIATED CONTENT

Supporting Information

The Supporting Information is available free of charge at https://pubs.acs.org/doi/10.1021/acsami.0c00891.

Experimental method for the synthesis of probes; equations for calculating the changes of fluorescence intensity; EDS of La(III)-MOF and La(III)-MOF-G and FESEM of La(III)-MOF-G; FT-IR spectra of La(III)-MOF and La(III)-MOF-G; UV−vis spectra of Ag NPs and Ag NPs−P2; fluorescence intensity changes of La(III)-MOF before and after modification with the aptamer (P1); comparison of the fluorescence intensity of La(III)-MOF, aptamer (P1), aptamer (P2), and miRNA-155; fluorescence intensity of the system in different conditions; spectral overlap between probes and changes of fluorescence intensity in the presence and absence of the quencher; and emission spectra of the biosensor containing various concentrations of miRNA-155 (PDF)

AUTHOR INFORMATION

Corresponding Author

Mahdi Mirzaee − *Faculty of Chemistry, Shahrood University of Technology, Shahrood 3619995161, Iran;* orcid.org/0000-0003-4093-8944; Email: mmirzaee@shahroodut.ac.ir

Author

Ahmad Afzalinia − *Faculty of Chemistry, Shahrood University of Technology, Shahrood 3619995161, Iran*

Complete contact information is available at: https://pubs.acs.org/10.1021/acsami.0c00891

Notes

The authors declare no competing financial interest.

ACKNOWLEDGMENTS

This work was financially supported by the Vice President's office for the research affairs of the Shahrood University of Technology. Also, the authors would like to thank the hematology and oncology center of Kousar hospital (Semnan, Iran) for the donation of the real samples.

REFERENCES

(1) Choi, Y.-E.; Kwak, J.-W.; Park, J. W. Nanotechnology for Early Cancer Detection. *Sensors* **2010**, *10*, 428−455.

(2) Chinen, A. B.; Guan, C. M.; Ferrer, J. R.; Barnaby, S. N.; Merkel, T. J.; Mirkin, C. A. Nanoparticle Probes for the Detection of Cancer Biomarkers, Cells, and Tissues by Fluorescence. *Chem. Rev.* **2015**, *115*, 10530−10574.

(3) Bharali, D. J.; Mousa, S. A. Emerging Nanomedicines for Early Cancer Detection and Improved Treatment: Current Perspective and Future Promise. *Pharmacol. Ther.* **2010**, *128*, 324−335.

(4) Mehrotra, P. Biosensors and Their Applications−A Review. *J. Oral Microbiol. Craniofac. Res.* **2016**, *6*, 153−159.

(5) Mittal, S.; Kaur, H.; Gautam, N.; Mantha, A. K. Biosensors for Breast Cancer Diagnosis: A Review of Bioreceptors, Biotransducers and Signal Amplification Strategies. *Biosens. Bioelectron.* **2017**, *88*, 217−231.

(6) Wang, B.; Akiba, U.; Anzai, J.-i. Recent Progress in Nanomaterial-Based Electrochemical Biosensors for Cancer Ciomarkers: A Review. *Molecules* **2017**, *22*, 1048.

(7) Jayanthi, V. S. P. K. S. A.; Das, A. B.; Saxena, U. Recent Advances in Biosensor Development for The Detection of Cancer Biomarkers. *Biosens. Bioelectron.* **2017**, *91*, 15−23.

(8) Pritchard, C. C.; Kroh, E.; Wood, B.; Arroyo, J. D.; Dougherty, K. J.; Miyaji, M. M.; Tait, J. F.; Tewari, M. Blood Cell Origin of Circulating MicroRNAs: A Cautionary Note for Cancer Biomarker Studies. *Cancer Prev. Res.* **2012**, *5*, 492−497.

(9) Harpio, R.; Einarsson, R. S100 Proteins as Cancer Biomarkers with Focus on S100B in Malignant Melanoma. *Clin. Biochem.* **2004**, *37*, 512−518.

(10) Asiago, V. M.; Alvarado, L. Z.; Shanaiah, N.; Gowda, G. A. N.; Owusu-Sarfo, K.; Ballas, R. A.; Raftery, D. Early Detection of Recurrent Breast Cancer Using Metabolite Profiling. *Cancer Res.* **2010**, *70*, 8309−8318.

(11) Reddy, K. B. MicroRNA (miRNA) in Cancer. *Cancer Cell Int.* **2015**, *15*, 38.

(12) Causa, F.; Aliberti, A.; Cusano, A. M.; Battista, E.; Netti, P. A. Supramolecular Spectrally Encoded Microgels with Double Strand Probes for Absolute and Direct miRNA Fluorescence Detection at High Sensitivity. *J. Am. Chem. Soc.* **2015**, *137*, 1758−1761.

(13) Fan, Y.; Chen, X.; Trigg, A. D.; Tung, C.-h.; Kong, J.; Gao, Z. Detection of MicroRNAs Using Target-Guided Formation of Conducting Polymer Nanowires in Nanogaps. *J. Am. Chem. Soc.* **2007**, *129*, 5437−5443.

(14) Iorio, M. V.; Ferracin, M.; Liu, C.-G.; Veronese, A.; Spizzo, R.; Sabbioni, S.; Magri, E.; Pedriali, M.; Fabbri, M.; Campiglio, M.; Ménard, S.; Palazzo, J. P.; Rosenberg, A.; Musiani, P.; Volinia, S.; Nenci, I.; Calin, G. A.; Querzoli, P.; Negrini, M.; Croce, C. M. MicroRNA Gene Expression Deregulation in Human Breast Cancer. *Cancer Res.* **2005**, *65*, 7065−7070.

(15) Liu, W.; Chen, A.; Li, S.; Peng, K.; Chai, Y.; Yuan, R. Perylene Derivative/Luminol Nanocomposite as a Strong Electrochemiluminescence Emitter for Construction of an Ultrasensitive MicroRNA Biosensor. *Anal. Chem.* **2018**, *91*, 1516−1523.

(16) Kilic, T.; Erdem, A.; Ozsoz, M.; Carrara, S. MicroRNA Biosensors: Opportunities and Challenges Among Conventional and Commercially Available Techniques. *Biosens. Bioelectron.* **2018**, *99*, 525−546.

(17) Lodes, M. J.; Caraballo, M.; Suciu, D.; Munro, S.; Kumar, A.; Anderson, B. Detection of Cancer with Serum miRNAs on an Oligonucleotide Microarray. *PLoS One* **2009**, *4*, No. e6229.

(18) Varkonyi-Gasic, E.; Wu, R.; Wood, M.; Walton, E. F.; Hellens, R. P. Protocol: a Highly Sensitive RT-PCR Method for Detection and Quantification of MicroRNAs. *Plant Methods* **2007**, *3*, 12.
(19) Várallyay, É.; Burgyán, J.; Havelda, Z. MicroRNA Detection by Northern Blotting Using Locked Nucleic Acid Probes. *Nat. Protoc.* **2008**, *3*, 190.
(20) Tian, T.; Wang, J.; Zhou, X. A Review: MicroRNA Detection Methods. *Org. Biomol. Chem.* **2015**, *13*, 2226−2238.
(21) Zhou, W.; Tian, Y.-F.; Yin, B.-C.; Ye, B.-C. Simultaneous Surface-Enhanced Raman Spectroscopy Detection of Multiplexed MicroRNA Biomarkers. *Anal. Chem.* **2017**, *89*, 6120−6128.
(22) Campuzano, S.; Pedrero, M.; Pingarrón, J. M. Electrochemical Genosensors for The Detection of Cancer-Related miRNAs. *Anal. Bioanal. Chem.* **2014**, *406*, 27−33.
(23) Asadi, H.; Ramasamy, R. P. In *Electrochemical Detection of Micro-RNAs as Potential Cancer Biomarker*, Meeting Abstracts; The Electrochemical Society, 2019; p 2275.
(24) Zhu, C.-s.; Zhu, L.; Tan, D.-a.; Qiu, X.-y.; Liu, C.-y.; Xie, S.-s.; Zhu, L.-y. Avenues Toward microRNA Detection In Vitro: A Review of Technical Advances and Challenges. *Comput. Struct. Biotechnol. J.* **2019**, *17*, 904−916.
(25) Wu, X.; Chai, Y.; Zhang, P.; Yuan, R. An Electrochemical Biosensor for Sensitive Detection of MicroRNA-155: Combining Target Recycling with Cascade Catalysis for Signal Amplification. *ACS Appl. Mater. Interfaces* **2015**, *7*, 713−720.
(26) Chang, J.; Wang, X.; Wang, J.; Li, H.; Li, F. Nucleic Acid-Functionalized Metal−Organic Framework-Based Homogeneous Electrochemical Biosensor for Simultaneous Detection of Multiple Tumor Biomarkers. *Anal. Chem.* **2019**, *91*, 3604−3610.
(27) Zhang, H.; Wang, Y.; Zhao, D.; Zeng, D.; Xia, J.; Aldalbahi, A.; Wang, C.; San, L.; Fan, C.; Zuo, X.; Mi, X. Universal Fluorescence Biosensor Platform Based on Graphene Quantum Dots and Pyrene-Functionalized Molecular Beacons for Detection of MicroRNAs. *ACS Appl. Mater. Interfaces* **2015**, *7*, 16152−16156.
(28) Yang, L.; Liu, C.; Ren, W.; Li, Z. Graphene Surface-Anchored Fluorescence Sensor for Sensitive Detection of MicroRNA Coupled with Enzyme-Free Signal Amplification of Hybridization Chain Reaction. *ACS Appl. Mater. Interfaces* **2012**, *4*, 6450−6453.
(29) Šípová, H.; Homola, J. Surface Plasmon Resonance Sensing of Nucleic Acids: A Review. *Anal. Chim. Acta* **2013**, *773*, 9−23.
(30) Crawford, B. M.; Strobbia, P.; Wang, H.-N.; Zentella, R.; Boyanov, M. I.; Pei, Z.-M.; Sun, T.-P.; Kemner, K. M.; Vo-Dinh, T. Plasmonic Nanoprobes for in Vivo Multimodal Sensing and Bioimaging of MicroRNA within Plants. *ACS Appl. Mater. Interfaces* **2019**, *11*, 7743−7754.
(31) Roda, A.; Mirasoli, M.; Michelini, E.; Di Fusco, M.; Zangheri, M.; Cevenini, L.; Roda, B.; Simoni, P. Progress in Chemical Luminescence-Based Biosensors: A Critical Review. *Biosens. Bioelectron.* **2016**, *76*, 164−179.
(32) Dehghani, S.; Nosrati, R.; Yousefi, M.; Nezami, A.; Soltani, F.; Taghdisi, S. M.; Abnous, K.; Alibolandi, M.; Ramezani, M. Aptamer-Based Biosensors and Nanosensors for The Detection of Vascular Endothelial Growth Factor (VEGF): A Review. *Biosens. Bioelectron.* **2018**, *110*, 23−37.
(33) Chen, Y.-X.; Huang, K.-J.; Niu, K.-X. Recent Advances in Signal Amplification Strategy Based on Oligonucleotide and Nanomaterials for MicroRNA Detection-A Review. *Biosens. Bioelectron.* **2018**, *99*, 612−624.
(34) Krishnan, S. K.; Singh, E.; Singh, P.; Meyyappan, M.; Nalwa, H. S. A Review on Graphene-Based Nanocomposites for Electrochemical and Fluorescent Biosensors. *RSC Adv.* **2019**, *9*, 8778−8881.
(35) Goryacheva, O. A.; Vostrikova, A. M.; Kokorina, A. A.; Mordovina, E. A.; Tsupka, D. V.; Bakal, A. A.; Markin, A. V.; Shandilya, R.; Mishra, P. K.; Beloglazova, N. V.; Goryacheva, I. Y. Luminescent Carbon Nanostructures for MicroRNA Detection. *TrAC, Trends Anal. Chem.* **2019**, *119*, 115613.
(36) Goryacheva, O. A.; Mishra, P. K.; Goryacheva, I. Y. Luminescent Quantum Dots for miRNA Detection. *Talanta* **2018**, *179*, 456−465.
(37) Cui, Y.; Chen, B.; Qian, G. Lanthanide Metal-Organic Frameworks for Luminescent Sensing and Light-Emitting Applications. *Coord. Chem. Rev.* **2014**, *273*−*274*, 76−86.
(38) Zhang, Y.; Yuan, S.; Day, G.; Wang, X.; Yang, X.; Zhou, H.-C. Luminescent Sensors Based on Metal-Organic Frameworks. *Coord. Chem. Rev.* **2018**, *354*, 28−45.
(39) Zhang, S.-Y.; Shi, W.; Cheng, P.; Zaworotko, M. J. A Mixed-Crystal Lanthanide Zeolite-like Metal−Organic Framework as a Fluorescent Indicator for Lysophosphatidic Acid, a Cancer Biomarker. *J. Am. Chem. Soc.* **2015**, *137*, 12203−12206.
(40) Wu, S.; Lin, Y.; Liu, J.; Shi, W.; Yang, G.; Cheng, P. Rapid Detection of The Biomarkers for Carcinoid Tumors by A Water Stable Luminescent Lanthanide Metal−Organic Framework Sensor. *Adv. Funct. Mater.* **2018**, *28*, 1707169.
(41) Meng, H.-M.; Shi, X.; Chen, J.; Gao, Y.; Qu, L.; Zhang, K.; Zhang, X.-B.; Li, Z. DNA Amplifier-Functionalized Metal−Organic Frameworks for Multiplexed Detection and Imaging of Intracellular mRNA. *ACS Sens.* **2020**, *5*, 103−109.
(42) Cui, Y.; Zhang, J.; He, H.; Qian, G. Photonic Functional Metal−Organic Frameworks. *Chem. Soc. Rev.* **2018**, *47*, 5740−5785.
(43) Liu, J.; Chen, L.; Cui, H.; Zhang, J.; Zhang, L.; Su, C.-Y. Applications of Metal−Organic Frameworks in Heterogeneous Supramolecular Catalysis. *Chem. Soc. Rev.* **2014**, *43*, 6011−6061.
(44) Kuppler, R. J.; Timmons, D. J.; Fang, Q.-R.; Li, J.-R.; Makal, T. A.; Young, M. D.; Yuan, D.; Zhao, D.; Zhuang, W.; Zhou, H.-C. Potential Applications of Metal-Organic Frameworks. *Coord. Chem. Rev.* **2009**, *253*, 3042−3066.
(45) Hu, Z.; Deibert, B. J.; Li, J. Luminescent Metal−Organic Frameworks for Chemical Sensing and Explosive Detection. *Chem. Soc. Rev.* **2014**, *43*, 5815−5840.
(46) Rieter, W. J.; Taylor, K. M. L.; Lin, W. Surface Modification and Functionalization of Nanoscale Metal-Organic Fframeworks for Controlled Release and Luminescence Sensing. *J. Am. Chem. Soc.* **2007**, *129*, 9852−9853.
(47) Zhu, X.; Zheng, H.; Wei, X.; Lin, Z.; Guo, L.; Qiu, B.; Chen, G. Metal−Organic Framework (MOF): A Novel Sensing Platform for Biomolecules. *Chem. Commun.* **2013**, *49*, 1276−1278.
(48) Meng, H.-M.; Liu, H.; Kuai, H.; Peng, R.; Mo, L.; Zhang, X.-B. Aptamer-Integrated DNA Nanostructures for Biosensing, Bioimaging and Cancer Therapy. *Chem. Soc. Rev.* **2016**, *45*, 2583−2602.
(49) Guo, X. Surface Plasmon Resonance Based Biosensor Technique: A Review. *J. Biophotonics* **2012**, *5*, 483−501.
(50) Miao, X.; Cheng, Z.; Ma, H.; Li, Z.; Xue, N.; Wang, P. Label-Free Platform for MicroRNA Detection Based on The Fluorescence Quenching of Positively Charged Gold Nanoparticles to Silver Nanoclusters. *Anal. Chem.* **2017**, *90*, 1098−1103.
(51) Hill, W. J.; Hunter, W. G. A Review of Response Surface Methodology: A Literature Survey. *Technometrics* **1966**, *8*, 571−590.
(52) Luo, Y.; Calvez, G.; Freslon, S.; Daiguebonne, C.; Roisnel, T.; Guillou, O. A Ffamily of Lanthanide-Containing Molecular Open Frameworks with High Porosity:[Ln (abdc)(Habdc), nH2O]∞ with Ln= La−Eu and 8≤ n≤ 11. *Inorg. Chim. Acta* **2011**, *368*, 170−178.
(53) Billaud, P.; Huntzinger, J.-R.; Cottancin, E.; Lermé, J.; Pellarin, M.; Arnaud, L.; Broyer, M.; Del Fatti, N.; Vallée, F. Optical Extinction Spectroscopy of Single Silver Nanoparticles. *Eur. Phys. J. D* **2007**, *43*, 271−274.
(54) Dao, X.-Y.; Guo, J.-H.; Wei, Y.-P.; Guo, F.; Liu, Y.; Sun, W.-Y. Solvent-Free Photoreduction of CO2 to CO Catalyzed by Fe-MOFs with Superior Selectivity. *Inorg. Chem.* **2019**, *58*, 8517−8524.
(55) Le Ru, E.; Etchegoin, P. *Principles of Surface-Enhanced Raman Spectroscopy: and Related Plasmonic Effects*; Elsevier, 2008.
(56) Zheng, Y.; Li, Y.; Deng, Z. Silver Nanoparticle−DNA Bionanoconjugates Bearing A Discrete Number of DNA Ligands. *Chem. Commun.* **2012**, *48*, 6160−6162.
(57) Giri, R. Temperature Effect Study Upon The Fluorescence Emission of Substituted Coumarins. *Spectrochim. Acta, Part A* **1992**, *48*, 843−848.
(58) Borghei, Y.-S.; Hosseini, M.; Ganjali, M. R.; Hosseinkhani, S. Label-Free Fluorescent Detection of MicroRNA-155 Based on

https://dx.doi.org/10.1021/acsami.0c00891
ACS Appl. Mater. Interfaces XXXX, XXX, XXX−XXX

Synthesis of Hairpin DNA-Templated Copper Nanoclusters by Etching (Top-Down Approach). *Sens. Actuators, B* **2017**, *248*, 133−139.
(59) Wu, X.; Chai, Y.; Yuan, R.; Su, H.; Han, J. A novel label-free electrochemical microRNA Biosensor Using Pd Nanoparticles as Enhancer and Linker. *Analyst* **2013**, *138*, 1060−1066.
(60) Liu, L.; Zhu, S.; Wei, Y.; Liu, X.; Jiao, S.; Yang, J. Ultrasensitive Detection of miRNA-155 Based on Controlled Fabrication of AuNPs@ MoS_2 Nanostructures by Atomic Layer Deposition. *Biosens. Bioelectron.* **2019**, *144*, 111660.
(61) Wang, F.; Fu, C.; Huang, C.; Li, N.; Wang, Y.; Ge, S.; Yu, J. Based Closed Au-Bipolar Electrode Electrochemiluminescence Sensing Platform for The Detection of miRNA-155. *Biosens. Bioelectron.* **2020**, *150*, 111917.
(62) Borghei, Y.-S.; Hosseini, M.; Ganjali, M. R. Fluorescence Based Turn-On Strategy for Determination of MicroRNA-155 Using DNA-Templated Copper Nanoclusters. *Microchim. Acta* **2017**, *184*, 2671−2677.
(63) Miao, X.; Cheng, Z.; Ma, H.; Li, Z.; Xue, N.; Wang, P. Label-Free Platform for MicroRNA Detection Based on the Fluorescence Quenching of Positively Charged Gold Nanoparticles to Silver Nanoclusters. *Anal. Chem.* **2018**, *90*, 1098−1103.
(64) Wei, J.; Ren, J.; Liu, J.; Meng, X.; Ren, X.; Chen, Z.; Tang, F. An Eco-Friendly, Simple, and Sensitive Fluorescence Biosensor for The Detection of Choline and Acetylcholine Based on C-Dots and The Fenton Reaction. *Biosens. Bioelectron.* **2014**, *52*, 304−309.
(65) Liu, L.-L.; Yu, Y.-Z.; Zhao, X.-J.; Wang, Y.-R.; Cheng, F.-Y.; Zhang, M.-K.; Shu, J.-J.; Liu, L. A robust Zn (ii)/Na (i)-MOF Decorated with [(OAc) 2 (H 2 O) 2] n 2n− Anions for The Luminescence Sensing of Copper Ions Based on The Inner Filter Effect. *Dalton Trans.* **2018**, *47*, 7787−7794.
(66) Zu, F.; Yan, F.; Bai, Z.; Xu, J.; Wang, Y.; Huang, Y.; Zhou, X. The Quenching of The Fluorescence of Carbon Dots: A Review on Mechanisms and Applications. *Microchim. Acta* **2017**, *184*, 1899−1914.
(67) Yang, Y.; Zou, T.; Wang, Z.; Xing, X.; Peng, S.; Zhao, R.; Zhang, X.; Wang, Y. The Fluorescent Quenching Mechanism of N and S Co-Doped Graphene Quantum Dots with Fe3+ and Hg2+ Ions and Their Application as a Novel Fluorescent Sensor. *Nanomaterials* **2019**, *9*, 738.
(68) Zeng, D.; Wang, Z.; Meng, Z.; Wang, P.; San, L.; Wang, W.; Aldalbahi, A.; Li, L.; Shen, J.; Mi, X. DNA Tetrahedral Nanostructure-Based Electrochemical miRNA Biosensor for Simultaneous Detection of Multiple miRNAs in Pancreatic Carcinoma. *ACS Appl. Mater. Interfaces* **2017**, *9*, 24118−24125.
(69) Erbes, T.; Hirschfeld, M.; Rücker, G.; Jaeger, M.; Boas, J.; Iborra, S.; Mayer, S.; Gitsch, G.; Stickeler, E. Feasibility of Urinary MicroRNA Detection in Breast Cancer Patients and Its Potential as An Innovative Non-Invasive Biomarker. *BMC Cancer* **2015**, *15*, 193.

https://dx.doi.org/10.1021/acsami.0c00891
ACS Appl. Mater. Interfaces XXXX, XXX, XXX−XXX